Global Change Biology

Global Change Biology (2012), doi: 10.1111/j.1365-2486.2012.02668.x

Description and quantification of pteropod shell dissolution: a sensitive bioindicator of ocean acidification

NINA BEDNARŠEK*†‡, GERAINT A TARLING*, DOROTHEE CE BAKKER†, SOPHIE FIELDING*, ANNE COHEN§, ALAN KUZIRIAN¶, DAN MCCORKLE§, BERTRAND LÉZÉ† and ROBERTO MONTAGNA†

*British Antarctic Survey, High Cross, Madingley Road, Cambridge, CB3 0ET, UK, †School of Environmental Sciences, University of East Anglia Research Park, Norwich, NR4 7TJ, UK, ‡University of Nova Gorica, Laboratory for Environmental Research, Vipavska 13, Rožna Dolina, Nova Gorica, 5000, Slovenia, §Woods Hole Oceanographic Institution, Department of Geology and Geophysics, 266 Woods Hole Road, Woods Hole, MA 02543, USA, ¶Marine Biological Laboratory, 7 MBL Street, Woods Hole, Woods Hole, MA 02543, USA

Abstract

Anthropogenic ocean acidification is likely to have negative effects on marine calcifying organisms, such as shelled pteropods, by promoting dissolution of aragonite shells. Study of shell dissolution requires an accurate and sensitive method for assessing shell damage. Shell dissolution was induced through incubations in CO_2-enriched seawater for 4 and 14 days. We describe a procedure that allows the level of dissolution to be assessed and classified into three main types: Type I with partial dissolution of the prismatic layer; Type II with exposure of underlying crossed-lamellar layer, and Type III, where crossed-lamellar layer shows signs of dissolution. Levels of dissolution showed a good correspondence to the incubation conditions, with the most severe damage found in specimens held for 14 days in undersaturated condition ($\Omega \sim 0.8$). This methodology enables the response of small pelagic calcifiers to acidified conditions to be detected at an early stage, thus making pteropods a valuable bioindicator of future ocean acidification.

Keywords: aragonite shell, bioindicator, dissolution quantification, ocean acidification, pteropods, shell dissolution

Received 25 January 2012; revised version received 25 January 2012 and accepted 1 February 2012

Introduction

Modelling the ocean-carbon cycle under the 'business-as-usual' IS92a scenario, aragonite undersaturation is predicted for the Southern Ocean surface waters by 2100 as a result of anthropogenic ocean acidification (Caldeira & Wickett, 2003; Orr *et al.*, 2005) and possibly sooner in wintertime (McNeil & Matear, 2008). Pteropods are likely to be the first indicators of where ocean acidification is starting to impact high-latitude pelagic marine communities as they are one of the few pelagic organisms to make their shells entirely out aragonite, a relatively soluble form of calcium carbonate (Fabry *et al.*,2008; Orr *et al.*, 2005).

Ocean acidification, and the modifications it induces to carbonate chemistry, will impact the shells of pelagic calcifiers in two ways. First, it will alter the ability of the organism to calcify and secondly, it will dissolve the calcified shell. In terms of calcification, Comeau *et al.* (2010) found that a decrease in saturation of aragonite in seawater (Ω) decreased the level of calcification in pteropod shells (*Limacina helicina*) significantly, although some calcification still occurred at relatively low levels of saturation. From these results, Comeau *et al.* (2012) predicted that *L. helicina* will become unable to precipitate $CaCO_3$ over much of the Arctic by the end of the century under the IPCC SRES A2 scenario. Also, such predictions do not take into account the effect of aragonite undersaturation on shell dissolution, which may act to accelerate the vulnerability of pelagic calcifiers. For instance, in a pilot study, Orr *et al.* (2005) noted significant corrosion to the shells of the pteropod *Clio pyramidata* incubated in water undersaturated for aragonite for 48 h.

Shell dissolution has been used as a useful indicator of aragonite undersaturation horizon ($\Omega < 1$) in sedimentary studies. For example, Ruddiman & Heezen (1967) determined the percentage of the non-carbonate vs. carbonate material to assess dissolution. Almogi-Labin *et al.* (1986) examined changes on the surface of pteropods shells using light microscopy and categorized them into stages, from transparent, indicating an excellent state of preservation, to opaque/white, indicating corrosion. Opacity under light microscopes was also adopted as an index of aragonite dissolution by

Correspondence: Nina Bednaršek, tel. + 386 0 5331 5204, fax + 386 0 5331 5296, e-mail: nina.bednarsek@ung.si

Haddad & Droxler (1996), Gerhardt *et al.* (2000), Gerhardt & Henrich (2001), and Manno *et al.* (2006).

Each of the above methods was developed to assess effects on mainly dead organisms below the saturation horizon where levels of dissolution are substantial. However, the effects of modern-day ocean acidification are likely to be small and sub-lethal, probably involving minute changes to the shell-surface. In such instances, light microscopy may not show sufficient details to detect such changes and there is a need for more precise and sensitive assessment methods. Scanning electron microscopy (SEM) can provide the extra resolution required to carry out such assessments. Nevertheless, the vacuum environment of SEM may otherwise introduce artefacts unless appropriate preparation techniques are used. A particular hazard in studying shell microstructure with SEM is the fragility of the thin pteropod shell walls (Bé *et al.*, 1972). In the *Limacinadae* family, this microstructure consists of underlying thick cross-lamellar layers and an upper thin prismatic layer that is covered with an organic layer (periostracum; Fig. 1). It is particularly thin in juveniles and prone to mechanical damage that may contribute to errors in interpreting damage induced by dissolution. Furthermore, the periostracum must be removed before SEM analysis, as remnants of this layer prevent an accurate examination of the shell surface, or be misinterpreted as shell damage.

This article describes a method for preparing pteropod shells and analysing dissolution on them that is capable of fine resolution and sensitive to the fragility of the specimens. We show that the technique can reveal the processes involved in the dissolution of pteropod shells under acidified conditions. We further develop a standardized metric scheme with which to categorize different levels of dissolution damage. This scheme establishes a benchmark against which the dissolution status of different pteropod species and populations can be compared. Such information is essential for an informed debate on the threat to shelled pteropods by ocean acidification.

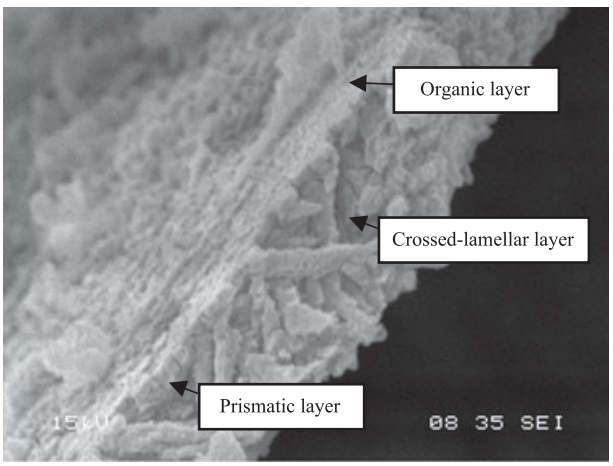

Fig. 1 SEM image illustrating the microstructure of the shelled pteropod L*imacina helicina antartica.* An organic layer covers a prismatic layer and an underlying crossed-lamellar crystal layer.

Materials and methods

Pteropod specimens were collected with slowly-hauled fine-meshed nets from various locations within the Scotia Sea, Southern Ocean (see Supplementary Information). Micro- and meso-zooplankton-sized specimens (mainly juveniles) were collected by vertically integrating the upper 200 m using a vertical Bongo (mesh size 200 μm with an opening of 0.5 m^2) and a towed Bongo net (2 nets, with 300 μm and 600 μm mesh sizes). Macrozooplankton-sized specimens (adults) were caught in RMT8 and RMT25 trawls (mesh size 4.5 mm). All the organisms used in incubations were alive at the start of the experiments, except for the natural control specimens that were preserved in 70% ethanol immediately. The majority of incubations were carried out on juvenile specimens for between 4 and 14 days at various Ω saturation levels. Mortality at the end of the experiments was low (<10%) and dead specimens were not considered further for SEM anaysis. As pteropods are prone to mechanical damage, a key factor when designing the incubation apparatus was to minimize physical interference. For this reason, closed blacked-out systems (2 L sealed borosilicate bottles) were used in which the water was enriched with CO_2 prior to incubation. Enrichment was achieved through the bubbling of different air/CO_2 mixtures (500 ppm, 750 ppm and 1200 ppm) through 0.7 μm filtered sea water until the required omega saturation level was reached. Omega was assessed from measurements of DIC (dissolved inorganic carbon) and total alkalinity (TA) at the start and end of each incubation experiment, which lasted 4, 8 or 14 days (see Supplementary Materials). Ω values were often different between incubation start and end points (up to ±0.17, Table 1), so only broad categorizations of incubation conditions were possible for comparative purposes, those being: (a) supersaturated ($\Omega > 1.2$) (b) transitional ($\Omega = 0.95$–1.2) and (c) Ω undersaturated ($\Omega < 0.95$; Table 1). The experiments with Ω supersaturated conditions lasted 8 days while transitional and Ω undersaturated experiments lasted 14 days. The incubation bottles were seeded with either live juveniles or adult *Limacina helicina antarctica* or adult *Clio pyramidata* forma *antarctica* and incubated for the set period, after which, they were preserved in 70% ethanol. Specimens were also extracted directly from the nets and preserved as above, so as to provide a control for incubation effects.

Shell preparation for SEM analysis (Fig. 2)

Shell preparation was performed in five major stages: (a) removal of abiogenic crystals from the shell surface, (b) dehydration,

Table 1 Conditions of incubations to which live juvenile pteropods were exposed (Ω supersaturation, $N = 9$; transitional state ($\Omega \sim 1$), $N = 11$ and Ω undersaturation for 4 and 14 days; $N = 11$). Incubations were performed in parallel. The values depict the mid-point between the values measured at the start and end of the incubation (± values depict the difference between the start and end measurements). Carbon chemistry parameters derived using Matlab CO_2sys, total pH scale, Mehrbach refit by Dickson and Millero

						Calculated parameters				
Experiment	Salinity	Phosphate (μmol/kg)	Silicate (μmol/kg)	Temp (°C)	TA (μmol/kg)	DIC (μmol/kg)	pH_T	pCO_2 (μatm)	HCO_3^- (μmol/kg)	CO_3^{2-} (μmol/kg)	Ω
Natural control	33.86	1.33	12.5	2.9	2290.6 ± 3.7	2123.0 ± 61.9	8.13 ± 0.13	318 ± 111	1983.1 ± 91.9	121.6 ± 39.6	1.82 ± 0.60
Supersaturation (experimental control) (8 days)	33.83	1.71	8.0	4.0	2360.3 ± 3.4	2211.5 ± 12.7	8.07 ± 0.03	387 ± 24	2077.8 ± 16.60	112.7 ± 5.4	1.70 ± 0.08
Transitional state	33.83	1.80	12.5	4.0	2316.8 ± 1.3	2245.0 ± 14.9	7.83 ± 0.05	690 ± 75	2144.7 ± 17.1	67.9 ± 6.3	1.03 ± 0.09
Undersaturation (4 days)	33.82	1.15	10.1	4.0	2323.1 ± 8.9	2295.5 ± 5.4	7.70 ± 0.01	940 ± 27	2192.7 ± 5.0	51.6 ± 1.8	0.78 ± 0.03
Undersaturation (14 days)	33.83	1.80	12.5	4.0	2330.3 ± 6.4	2298.3 ± 0.0	7.73 ± 0.01	883 ± 12	2191.0 ± 4.4	54.8 ± 0.90	0.83 ± 0.02

(c) mounting on the SEM stub, (d) removal of the organic layer and (e) sputter coating and SEM analysis.

Removing abiogenic crystals from the shell surface. At the time of sample collection from the field, pteropod samples were directly transferred from seawater to 70% ethanol. This resulted in the precipitation of various crystalline structures on the shell surface. To remove crystal deposits from the shell surface, the samples were transferred from 70% ethanol (in which they were kept from the time of sample collection) to 50% ethanol for 2–3 min. They were subsequently transferred to distilled water (3–5 min). Two different procedures for removing the precipitated crystals on pteropod shells were tested for their ease of use and efficiency. In the first method, hydrogen peroxide (H_2O_2) was used to dissolve the crystals. The hydrogen peroxide concentration and the exposure time were adjusted to maintain shell integrity. Samples were treated with two consecutive rinses in 6% H_2O_2 for 15–20 min. Alternatively, Triton-X-100 and slight sonication were used to dislodge surface material. The shells were put into 100–200 ml of 0.5% Triton-X-100 in seawater and sonicated for 5 s. The sonication procedure was repeated two to three times at 5 s each. In this study, we mainly used the first approach for abiogenic crystal removal, which we recommend for future use. Finally, all samples were washed twice in distilled water for a total of 5 min.

Dehydration. Dehydration was undertaken using 2,2-Dimethoxypropane (DMP; chemical formula: $(CH_3)_2C(OCH_3)_2$), and 1,1,1,3,3,3-hexamethyldisilazane [HMDS; chemical formula: $(CH_3)_3SiNHSi(CH_3)_3$]. Before starting dehydration with DMP, the shells were transferred to 50% methanol for two 5 min washes then transferred to 85% methanol (10 min). Complete tissue dehydration was accomplished by immersion in DMP: two changes at 15–20 min each. It was important not to let the shells air dry at this stage, so they were transferred to a 1 : 1 mixture of DMP and HMDS for about 10 min, followed by 100% HMDS for 20–25 min twice. The HMDS was subsequently allowed to evaporate allowing the shells to dry completely (Fig. 2). The moderate vapour pressure and very low surface tension of HMDS allowed the shells to dry without distortion or loss of shell integrity.

Mounting on the SEM stub. Fine brushes were used to mount the dry shells on aluminium SEM stubs using colloidal graphite. Extreme care was needed when manoeuvring the shell with a brush, as this could cause structural damage or even shell collapse. Shells had to be positioned in a dorso-ventral position for the oxygen plasma etching reaction (see below) to expose the maximum surface area, and for qualitative examination. To examine the changes on the growing edge, a proximo-distal position of the shell with the aperture on top was chosen.

Removal of the organic shell layer using oxygen plasma etching. The samples had to be completely dry and oriented to expose the maximum surface area prior to etching. A BIO-RAD RF plasma barrel etcher PT7150 was used with a

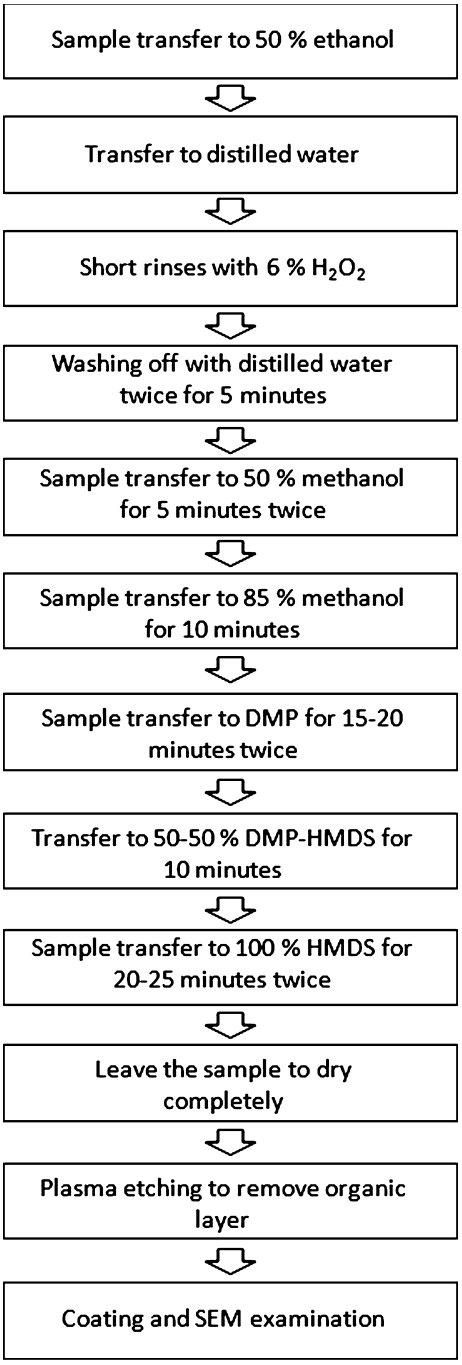

Fig. 2 Method for the shell preparation of juvenile *Limacina helicina antarctica* stored in 70% ethanol.

forward power of ≈200 Watts and a reflected power of ≈5 Watts. The shells were typically etched for between 10 and 30 min, depending on the power of the etcher.

Adult shells are less fragile than juvenile shells, hence less sensitive preparation procedures were sufficient. For instance, for rapid removal of abiogenic crystals, it was possible to use a stronger solution of hydrogen peroxide (30% H_2O_2). This concentration was also reasonably efficient at removing the periostracum, although it did not perform as well as the plasma etching. Two sequential immersions in 30% H_2O_2 for 10–12 min each were required to remove the abiogenic crystals and most of the overlying organics. Transfer to 100% HMDS for 25–30 min was sufficient for complete dehydration and drying.

Categorization scheme for pteropod shell dissolution

Analysis of the SEM photos enabled observation of the shell surface and identification of shell dissolution; notably pitting, cracks, and areas where aragonite crystals were absent or porous. Different stages in the level of dissolution were recognizable and so a scheme was devised that categorized these stages into three types (Types I, II, III), which are described in detail in a later section.

Application of scheme to incubated specimens

The categorization scheme above was applied in a semi-quantitative manner using image segmentation analysis to assess the extent of each dissolution type over the shell surface. Analyses were performed only on those pteropods that were successfully maintained in the experimental conditions, therefore excluding mortality as a factor of variability. Overall, 50 animals were examined; 20 animals from the natural environment, 9 from the supersaturated incubations, 11 from the transitional incubations ($\Omega \sim 1$), and 11 from the undersaturated incubations. For each individual, 15–20 SEM photographs were generated across the shell surface area, which amounted to a total of 750 SEM micrographs, on which image the segmentation analysis was performed. This procedure is described in Supplementary Materials. Statistical differences in dissolution levels between incubations were determined with a Kruskal-Wallis 1-way ANOVA on ranks followed by Dunn's Method to determine which pairwise differences were significantly different ($P < 0.05$).

Results and discussion

Shell preparation method

The shell preparation method proved to be non-destructive, providing specimens with clean and intact shell surfaces, thus limiting the occurrence of methodological artefacts and rendering an intact crystalline layer suitable for further SEM examination. Each of the steps is considered in further detail below:

Removal of abiogenic crystals and bacteria. The transfer of samples from seawater to 70% ethanol caused rapid water removal and the precipitation of phosphate, calcium and sodium chloride (NaCl) crystals on the shell surface. Without applying the shell preparation method, the crystals covered much of the shell surface,

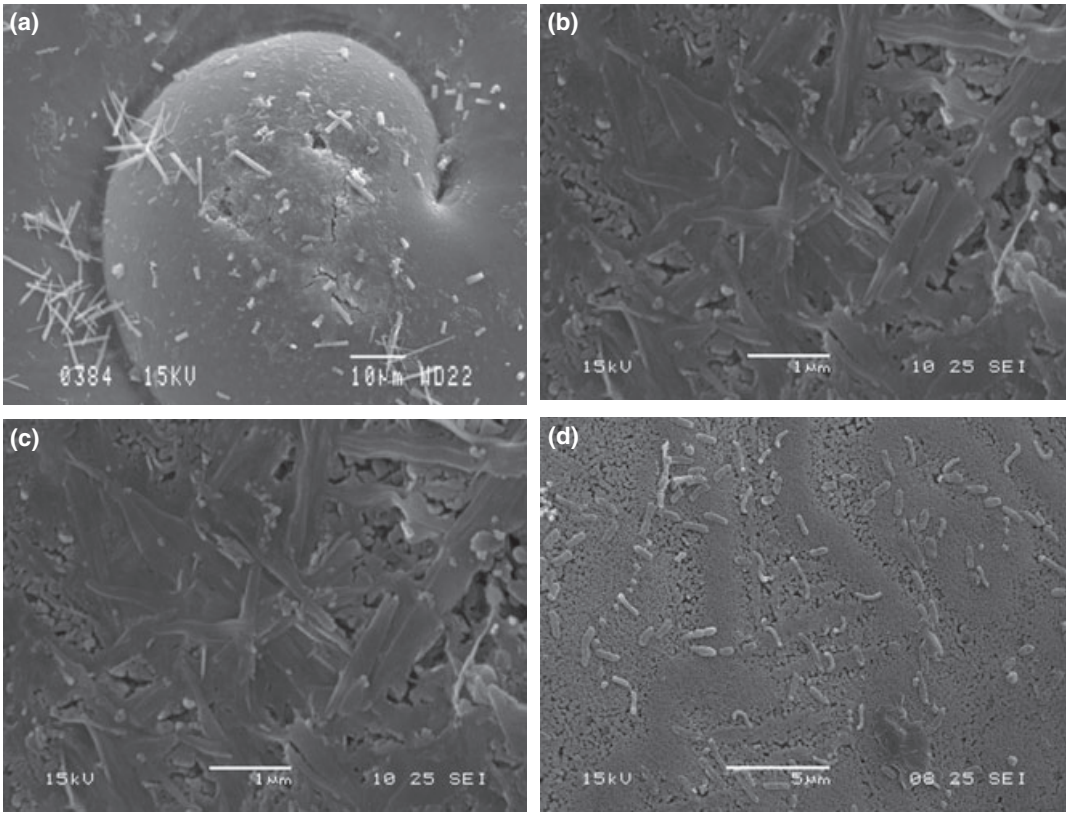

Fig. 3 Abiogenic precipitation and contamination with bacteria on the shell surface of juvenile and adult pteropods. (a) phosphate crystals in the struvite form (crystal rods) and NaCl salts (squares); (b) phosphate crystals in rosette form; (c) triple phosphate crystals; (d) bacterial contamination with phosphate crystals in rosette form.

and made it impossible to examine it for evidence of dissolution (Fig. 3 shows various abiogenic crystals). Phosphate crystals occurred in the struvite (Fig. 3a), rosette (Fig. 3b) or in triple phosphate forms (Fig. 3c). Sodium chloride formed cubes (Fig. 3b). In addition, bacteria from seawater attached to the surface and in some cases, completely covered the shell (Fig. 3d). Therefore, removal of abiogenic crystals with H_2O_2 was necessary before SEM examination.

An alternative approach to minimize or avoid the precipitation of abiogenic crystals on the shell surface during sample fixing would have been to place samples in a low ethanol grade (50%), followed by subsequent, transfer to higher concentrations (up to 70%) in gradual steps. This method allows dilution of the salts in the high concentrations of seawater and their subsequent removal. Samples should not be fixed in buffered formalin for dissolution studies, because formalin dissolves aragonite crystals.

Removal of the organic layer. Although extremely thin, the outer organic layer is fully embedded within the surface crystals of the shell. This periostracum must be removed before SEM examination for two reasons: (i) microstructural changes of the aragonite crystals can otherwise be obscured and (ii) disintegration of organic remnants during coating for SEM can lead to misinterpretation of dissolution in the subsequent analysis or obscure signs of shell dissolution. Juvenile shells are especially fragile and prone to mechanical damage and disintegration, thus an inappropriate method could easily damage these delicate shells. A common way to etch the surface of SEM samples is acid hydrolysis that denatures surface proteins and thus eliminates the periostracum. However, acid treatment is unsuitable for shell dissolution studies because it dissolves aragonite crystals. Therefore, oxygen plasma etching was found to be a non-destructive and efficient procedure for removing the periostracum from delicate pteropod shells.

Preparation artefacts. Drying of the samples and mounting them on SEM stubs were the steps with the greatest potential to cause mechanical damage to the shells. Despite taking the utmost care, mechanical damage

(e.g. cracks, pitting, broken growing edges) mostly originated from handling while mounting the samples on SEM stubs. It was, nevertheless, possible to distinguish this type of damage from the effects of dissolution when scrutinized under SEM. In addition, in shells that were not properly dehydrated, the vacuum force during coating for SEM resulted in the collapse of the organic matrix (Fig. 4a, b), and cracked and chipped growing edge (Fig. 4c) and pitted surfaces (Fig. 4d). Occasional damage to shells, particularly at the growing edge, occurred most frequently in juveniles that had been incubated in Ω undersaturated water, where dissolution had weakened the shells. Hence, it was important to dry fully and remove the organic layer prior to coating. DMP and HMDS were used to avoid these artefacts. DMP did not cause any deterioration or physical change to specimens (Maser & Trimble, 1977). HMDS dried the organic meshwork and stabilized the complex protein structures of the shell without changing or destroying any structural features. This was achieved by decreasing surface tensions during drying with HMDS; otherwise damage to fragile structures

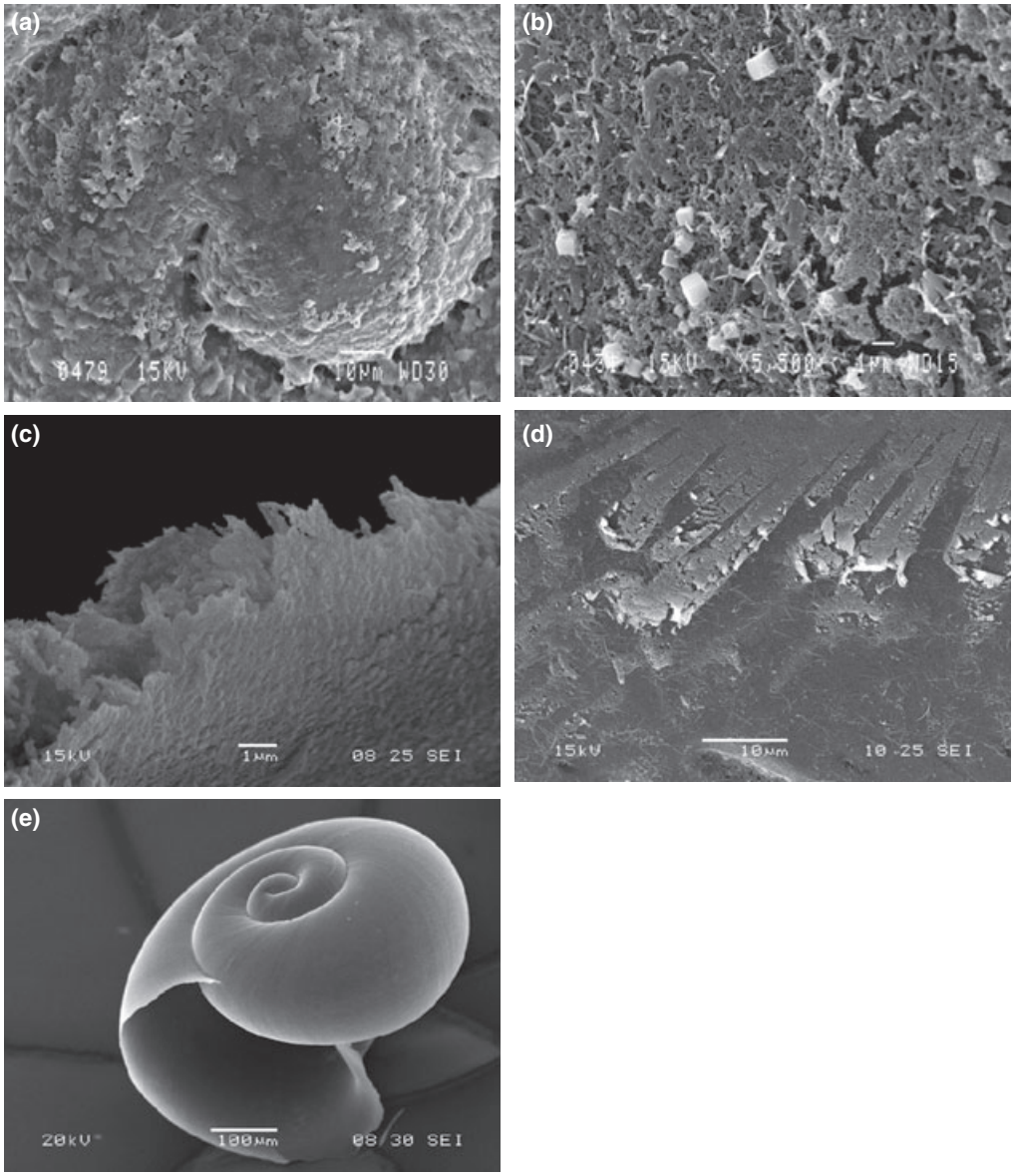

Fig. 4 Artefacts on shells of juvenile pteropods caused by inadequate shell preparation: (a, b) a partly collapsed organic matrix; (c) crushed and chipped growing edges generated by mechanical damage or high vacuum exposure; (d) pitted surfaces not caused by dissolution; (e) the correct shell preparation method leaves the shell and growing edge intact and, with the organic layer removed, the crystal structure is revealed.

within the shell would occur. HMDS is an inexpensive, easy to handle, and time-saving alternative to critical point drying.

The methodology used for live juveniles was equally effective for adult *L. helicina ant.* Adults were rare in our samples, but were easier to work with than juveniles, as they are larger to handle and their shells are more compact. This allowed certain preparation steps to be modified. For example, H_2O_2 could be applied in higher concentrations and for longer durations to remove the abiogenic crystal precipitation. This reduced or totally eliminated the time required to remove the organic layer by oxygen plasma etching. Additionally, dehydration steps could be shortened (for instance, through eliminating 85% methanol and double immersion in DMP), as long as the HMDS step was long enough to attain proper water removal.

The method also worked effectively for *C. pyramidata* f. *ant.*, despite differences in the shell structure compared with *L. helicina ant.* The shell microstructure of *C. pyramidata* f. *ant.* is helical with a prismatic layer that is a few microns thick and covered by a thin organic layer (Bé & Gilmer, 1977).

With the organic layer removed, the crystal structure of the prismatic layer was revealed (Fig. 4e). For samples exposed to high CO_2 levels, SEM observations revealed initial (Type I; Fig. 5), intermediate (Type II; Fig. 6) and advanced (Type III: Fig. 7) dissolution levels on the shell.

The process of dissolution and categorization scheme for shell dissolution

Dissolution of the aragonite crystals on the shell surface and growing edge was assessed by comparing SEM images of pteropods exposed to high CO_2 levels with those of controls. The progression of shell dissolution was divided into four stages based on the level of shell damage: No dissolution, and Types I, II and III (Table 2). A pteropod shell taken from ambient seawater with supersaturated conditions for omega typically had a smooth, sleek shell surface (Fig. 4e) and the shell structure was compact with very little intracrystalline porosity. Type I dissolution corresponded to a mild degree of dissolution defined by small effects on the upper prismatic layer and initial exposure of aragonite crystals. As a result of dissolution, intact heads of the aragonite crystals appeared as 'cauliflower heads' (Fig. 5a, b). There were only rare deep intrusions into the crossed-lamellar layer, but the shell had become porous, less compact, and hence more fragile than an intact shell.

The next level of dissolution was categorized as Type II dissolution. It was represented by the partial disappearance of the prismatic layer. The crossed-lamellar layer had been exposed, but not affected by dissolution (Fig. 6b). Progressive roughening of the shell surface induced by dissolution substantially enhanced the rate of shell dissolution, as first suggested by Acker & Byrne (1989). Shell porosity had increased, and the shell surface had numerous, large damaged patches across the shell surface (Fig. 6a).

As the dissolution process continued, an extended degree of porosity and dissolution of the crossed-lamellar layer was evident over the shell surface (Fig. 7b). In the case of Type III dissolution, the crystals of the crossed-lamellar layer had been partly eroded and became thicker and chunkier in appearance (Fig. 7c). As shell dissolution was extensive with a loosely organized crystal structure, shell integrity had been lost and the shell was prone to fragmentation and increased frailness (Fig. 7a).

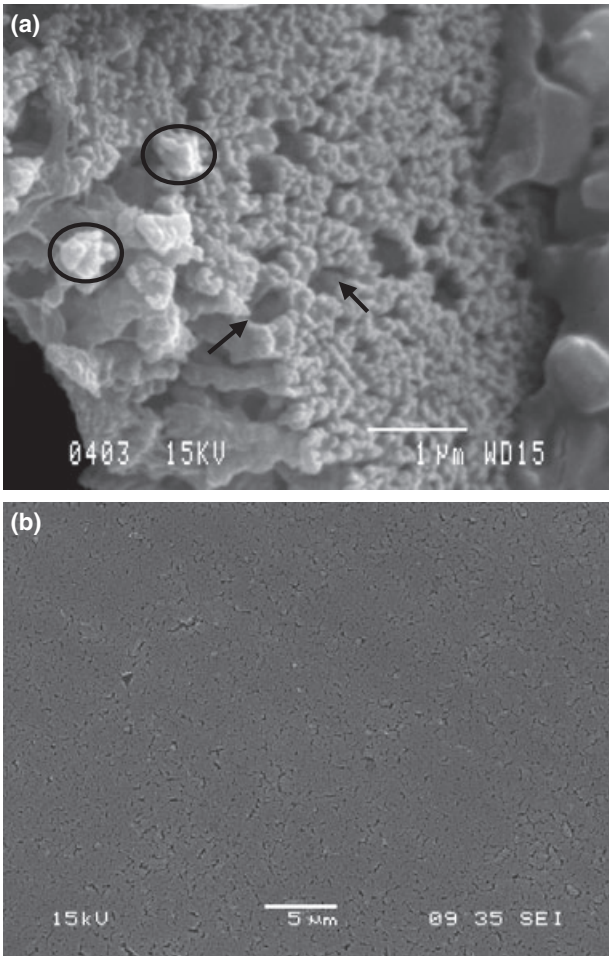

Fig. 5 Type I dissolution: Aragonite crystals are missing and 'cauliflower heads' have appeared (encircled) (a) the porosity has increased (b).

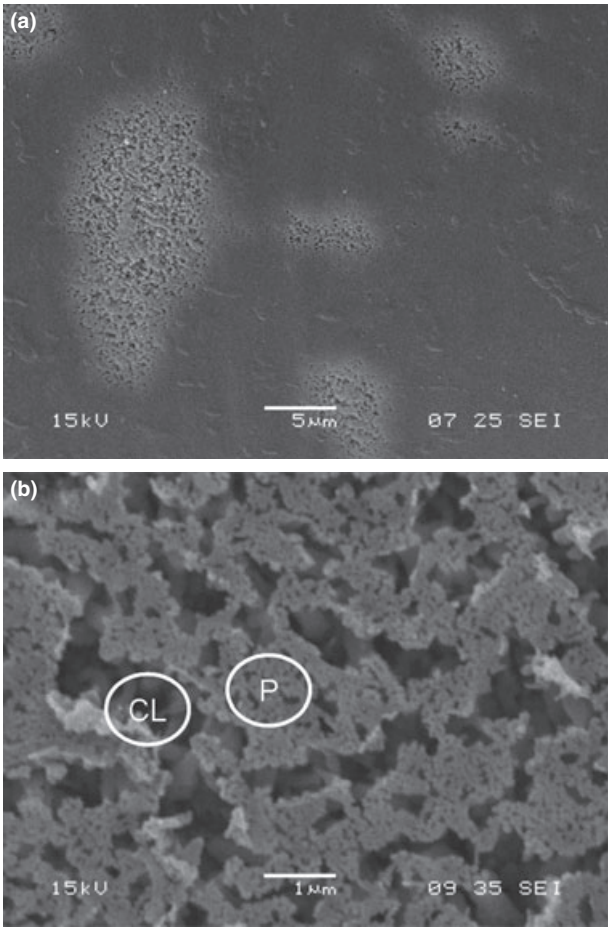

Fig. 6 Type II dissolution: Larger areas of the shell surface are covered by dissolved patches, where dissolution is penetrating deeper (a) affecting the prismatic (P) layer, and exposing the crossed-lamellar layer (CL) (b).

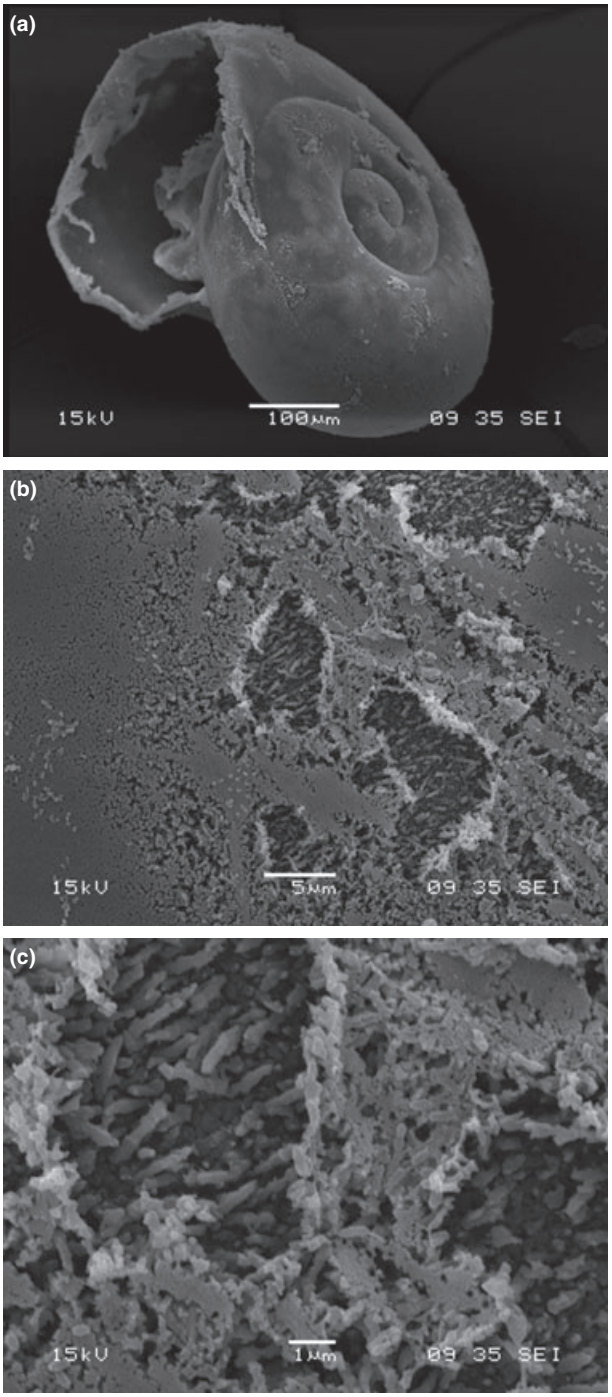

Fig. 7 Type III dissolution: Increased shell frailness (a) as a result of much of the shell surface being affected by dissolution (b) with extensive Type III dissolution causing large gaps in the prismatic layer and exposing the crossed-lamellar layer (c).

Dissolution at the growing edges

The dissolution categorization scheme for the shell surface was also applicable to the growing edge. At the onset of dissolution, the intact crystal structure (Fig. 8a) was replaced by 'cauliflower heads' indicating Type I dissolution (Fig. 8c). In the most severe cases, dissolution transformed the crystals from long aragonite rods present on an intact shell (Fig. 8b) to thick, short, loosely arranged crystals with eroded lateral edges of Type III dissolution (Fig. 8d). As a result, the growing edge had become less rigid and more fragile.

Semi-quantification of shell surface dissolution

Image segmentation allowed the extent of the three different categories of shell dissolution to be estimated in a semi-quantitative manner.

There were statistically significant differences in dissolution levels between natural and incubated specimens and also between different incubation treatments (Kruskall-Wallis 1-way ANOVA on Ranks, H = 29.15–

Table 2 Summary of the main features of each dissolution type

Dissolution type	Description	Ω value when first observed
Type I	• First indices of slightly increased porosity • Aragonite crystals within the upper-prismatic layer affected by dissolution - 'cauliflower heads' present	• In a small extent present in the natural environment • Widespread at decreased Ω supersaturation
Type II	• Increased porosity • Dissolved patches more extensive and numerous • Prismatic layer partially or completely dissolved, crossed-lamellar layer exposed	• In small extent present at transitional state; more common in undersaturated conditions
Type III	• Less compact crystal structure with compromised shell integrity and extreme frailness • Dissolution within crossed-lamellar layer with crystals thicker and chunkier	• At transitional Ω conditions; larger, more extensive patches in Ω undersaturated conditions, particularly with increased time of exposure

35.38, $P < 0.001$; Fig. 9). After incubation in supersaturated conditions (Ω ~ 1.65) for 8 days, roughly half of the shell surface was covered with Type I dissolution (Fig. 9). Given that very little dissolution was observed in natural field samples extracted from supersaturated ambient conditions, we considered such dissolution to be an incubation effect and used as a baseline with which to compare against other incubations.

Type I dissolution was also present on shells incubated in transitional conditions for 14 days, but covered 80% of the surface area of each shell (SD = 15) with a remaining 15% (SD = 10) covered with Type II dissolution. In shells incubated in undersaturated conditions for 4 days, Type II dissolution covered 26% of the shell (SD = 6; Fig. 9) and there was evidence of Type III dissolution, although only over 3% of the shell

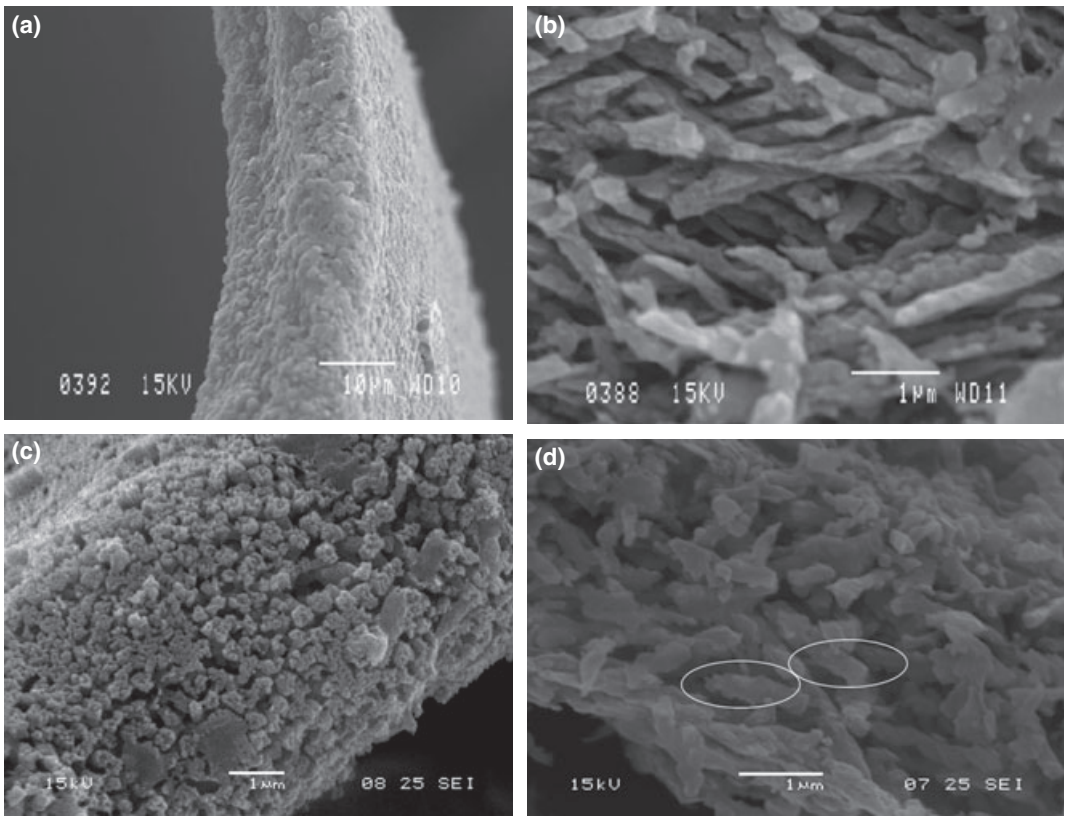

Fig. 8 The growing edge of juvenile pteropods: (a) intact growing edge covered by the organic layer; (b) intact crystals within crossed-lamellar layer of the growing edge; (c) Type I dissolution - increased porosity and appearance of 'cauliflower heads' in the prismatic layer; (d) Type III dissolution - aragonite crystals in the crossed-lamellar layer are thicker and shorter as a result of dissolution.

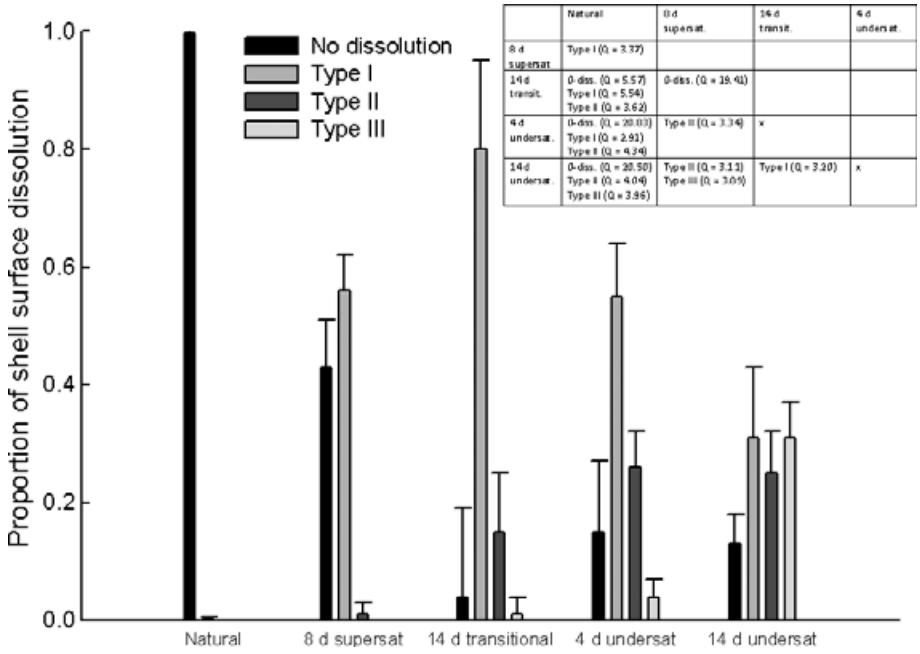

	Natural	8 d supersat.	14 d transit.	4 d undersat.
8 d supersat	Type I (Ω = 3.37)			
14 d transit.	0-diss. (Ω = 5.57) Type I (Ω = 5.54) Type II (Ω = 3.62)	0-diss. (Ω = 19.41)		
4 d undersat.	0-diss. (Ω = 20.03) Type I (Ω = 2.91) Type II (Ω = 4.34)	Type III (Ω = 3.34)	x	
14 d undersat.	0-diss. (Ω = 20.50) Type II (Ω = 4.04) Type III (Ω = 3.66)	Type III (Ω = 3.13) Type III (Ω = 3.05)	Type I (Ω = 3.20)	x

Fig. 9 Bar graph: Correspondence between the extent of dissolution and the Ω saturation state within incubations showing mean (SD) levels of dissolution according to environmental conditions (natural or incubated at different levels of Ω saturation). Matrix: dissolution types showing significant pairwise differences between treatments. 'x' denotes that no significant differences were found; '0-diss.' denotes no detectable dissolution.

surface (SD = 3). In specimens incubated for 14 days in conditions, Type III dissolution was present across one-third of the total shell surface (31% coverage, SD = 6; Fig. 9). The type and extent of dissolution were consistent across pteropods incubated in similar conditions as evidenced by the low standard deviations (Fig. 9).

The fact that Type I dissolution occurred when the organism was held in supersaturated conditions for 8 days and the organic layer was intact raises questions about the role of the organic layer as a protection against dissolution. Clark (1999) postulated that the organic layer would have to be severely altered or destroyed before the crystal structure of the shell would be affected by chemicals, i.e. acidic attack. Similarly, Vermeij (1993) regarded a thick periostracum as a molluscan adaptation for slowing down dissolution. A microstructure with a high organic content provides high resistance to dissolution by shrouding the crystals (Harper, 2000). However, while Glover & Kidwell (1993) regarded the organic layer as a protection against dissolution, they also acknowledged the possibility that the organic layer could enhance dissolution by promoting growth of acid-releasing microbes. We propose that the periostracum does not provide protection from acidified waters.

Altogether, the development of a reliable method by which to prepare pteropod shells for SEM analysis has allowed us to describe in detail the process of how shell-surface dissolution progresses from its initial stages to severe levels of damage. It has also allowed us to develop an easily applicable categorization scheme for types of shell dissolution and subsequently, a means of obtaining a semi-quantitative assessment of the extent of different types of dissolution on pteropod shells, with the assistance of some custom-made freeware for image segmentation analysis (see Supplementary Materials). With appropriate calibration, these developments will in turn allow levels of dissolution to be quantified and contribute to studies of oceanic carbon budgets. Establishing functional responses between aragonite saturation state and the extent of dissolution in pteropod shells is the next important step in this process. Such functions are an important aspect of considering not only the biogeochemical consequences of the dissolution of calcifiers but also their future viability in acidifying oceans. Based on their demonstrated response to subtle changes in carbonate chemistry, this study suggests that the monitoring of pteropod shell dissolution can serve not only as a proxi of saturation state in the past (Gerhardt & Henrich, 2001), but also as a sensitive bioindicator of modern day ocean acidification. Wider application will also increase our ability to assess the impact of these changes on other pelagic calcifiers.

Acknowledgements

We thank the officers and crew of the RRS James Clark Ross for their support during the cruise JR177, from which the live material was obtained and experiments were conducted. Thanks for help on SEM goes to Louis Kerr at MBL Central Microscopy Facility (CMF) and Bertrand Lézé at UEA. NB was supported by the FAASIS (Fellowships in Antarctic Air-Sea-Ice Science), a Marie Curie Early Stage Training Network with grant number MEST-CT-2004-514159. Part of the sample preparation, SEM imaging and analysis was conducted during NB's term as a vising student at the Woods Hole Oceanographic Institution with Anne Cohen and Daniel McCorkle. This component of the work was funded through grants from the WHOI Ocean Climate Change Institute and NSF OCE 1041106 to ALC and DCM. GT and SF carried out this work as part of the DISCOVERY 2010 and ECOSYSTEM programmes at BAS.

References

Acker JG, Byrne RH (1989) The influence of surface state and saturation state on the dissolution kinetics of biogenic aragonite in seawater. *American Journal of Science*, 289, **9**, 1098–1116.

Almogi-Labin A, Luz B, Duplessy DC (1986) Quaternary paleo-oceanography, pteropod preservation and stable-isotope record of the Red Sea. *Palaeogeography, Palaeoclimatology, Palaeoecology*, **52**, 195–211.

Bé AWH, Gilmer RW (1977) A zoogeographic and taxonomic review of euthecosomatous Pteropoda. In: *Oceanic Micropalaeontology I.* (ed. Ramsay ATS), pp. 733–808. Academic Press, London.

Bé AWH, MacClintock C, Currie DC (1972) Helical shell structure and growth of the pteropod *Cuvierina columnella* (Rang) (Mollusca, Gastropoda). *Biomineralization Research Reports*, **4**, 47–79.

Caldeira K, Wickett ME (2003) Anthropogenic carbon and ocean pH. *Nature*, **437**, 681–686.

Christoudias CM, Georgescu B, Meer P (2002) Synergism in low-level vision. *16th International Conference on Pattern Recognition*, **4**, 150–155.

Clark GR II (1999) Organic matrix taphonomy in some molluscan shell microstructures. *Palaeogeography, Palaeoclimatology, Palaeoecology*, **149**, 305–312.

Code for the Edge Detection and Image Segmentation System Center for Advanced Information Processing of Rutgers University, 2002. Available at: http://coewww.rutgers.edu/riul/resaearch/code/EDISON/index.html (accessed 19 October 2011).

Comaniciu D, Meer P (2003) "Mean shift: a robust approach toward feature space analysis." *IEEE Transactions on pattern analysis and machine intelligence*, **24**, 603–619.

Comeau S, Jeffree R, Teyssie JL *et al.* (2010) Response of the Arctic pteropod *Limacina helicina* to projected future environmental conditions. *PLoS ONE*, **5**, e11362.

Comeau S, Gattuso JP, Nisumaa AM *et al.* (2012) Impact of aragonite saturation state changes on migratory pteropods. *Proceedings of the Royal Society B Biological Sciences*, **279**, 732–738.

Dickson AG (1981) An exact definition of total alkalinity and a procedure for the estimation of alkalinity and total inorganic carbon from titration data. *Deep-Sea Research Part I. Oceanographic Research Papers*, **28**, 609–623.

Dickson AG, Millero FJ (1987) A comparison of the equilibrium constants for the dissociation of carbonic acid in seawater media. *Deep-Sea Research Part I. Oceanographic Research Papers*, **34**, 1733–1743.

Dickson AG, Sabine CL, Christian JR (2007) Guide to best practices for ocean CO_2 measurements. *PICES Special Publication*, **3**, 1–191.

Fabry VJ, Seibel BA, Feely RA *et al.* (2008) Impacts of ocean acidification on marine fauna and ecosystem processes. *ICES Journal of Marine Science*, **65**, 414–432.

Georgescu CM (2002) Synergism in low level vision. *16th International Conference on Pattern Recognition, Proceedings*, **4**, 150–155.

Gerhardt S, Henrich R (2001) Shell preservation of *Limacina inflata* (Pteropoda) in surface sediments from the Central and South Atlantic Ocean: a new proxy to determine the aragonite saturation state of water masses. *Deep Sea Research Part I. Oceanographic Research Papers*, **48**, 2051–2071.

Gerhardt S, Groth H, Rühlemann C *et al.* (2000) Aragonite preservation in late Quaternary sediment cores on the Brazilian Continental Slope: implications for intermediate water circulation. *International Journal of Earth Sciences*, **88**, 607–618.

Glover CP, Kidwell SM (1993) Influence of organic matrix on the post-mortem destruction of molluscan shells. *The Journal of Geology*, **101**, 729–747.

Haddad GA, Droxler AW (1996) Metastable $CaCO_3$ dissolution at intermediate water depths of the Caribbean and western North Atlantic: implications for intermediate water circulation during the past 200,000 years. *Paleoceanography*, **11**, 701–716.

Harper EM (2000) Are calcitic layers an effective adaptation against shell dissolution in the Bivalvia? *Journal of Zoology*, **251**, 179–186.

Johnson KM, Sieburth JM, Williams PJL, Brandstrom L (1987) Coulometric total carbon dioxide analysis for marine studies - automation and calibration. *Marine Chemistry*, **21**, 117–133.

Lewis E, Wallace DWR (1998) *CO2SYS-Program Developed for the CO_2 System Calculations, Report ORNL/CDIAC-105.* Carbon Dioxide Information Analysis Center, Oak Ridge National Laboratory, U.S. Department of Energy, Oak Ridge, Tennessee.

Manno C, Sandrini S, Tositti L *et al.* (2006) First stages of degradation of *Limacina helicina* shells observed above the aragonite chemical lysocline in Terra Nova Bay (Antarctica). *Journal of Marine Systems*, **68**, 91–102.

Maser MD, Trimble JJ (1977) Rapid chemical dehydration of biologic samples for scanning electron microscopy using 2, 2-dimethoxypropane. *Journal of Histochemistry and Cytochemistry*, **25**, 247–251.

McNeil BI, Matear RJ (2008) Southern Ocean acidification: a tipping point at 450-ppm atmospheric CO_2. *Proceedings of the National Academy of Sciences*, **105**, 18860–18864.

Mehrbach C, Culberson CH, Hawley JE *et al.* (1973) Measurement of the apparent dissociation constants of carbonic acid in seawater at atmospheric pressure. *Limnology and Oceanography*, **18**, 897–907.

Orr JC, Fabry VJ, Aumont O *et al.* (2005) Anthropogenic ocean acidification over the twenty-first century and its impact on calcifying organisms. *Nature*, **437**, 681–686.

Ruddiman WF, Heezen BC (1967) Differential solution of planktonic foraminifera. *Deep Sea Research and Oceanographic Abstract*, **14**, 801–808.

Vermeij GJ (1993) *A Natural History of Shells*, pp. 39–54. Princeton University Press, Princeton, NJ.

Wiebe PH, Morton AW, Bradley AM *et al.* (1985) New development in the MOCNESS, an apparatus for sampling zooplankton and micronekton. *Marine Biology*, **87**, 313–323.

Supporting Information

Additional Supporting Information may be found in the online version of this article:

Material S1. Supplementary material.

Please note: Wiley-Blackwell are not responsible for the content or functionality of any supporting materials supplied by the authors. Any queries (other than missing material) should be directed to the corresponding author for the article.